SPARC WORKING POINT OPTIMIZATION FOR A BUNCH WITH GAUSSIAN TEMPORAL PROFILE

M. Boscolo, M. Ferrario, V. Fusco, M. Migliorati, INFN-LNF, Frascati, Italy
C. Ronsivalle, ENEA-CR, Frascati, Italy
S. Reiche, UCLA Dept. of Physics/Astronomy, USA

Abstract

We present the optimization of the working point with a Gaussian temporal profile for the SPARC photoinjector. Start to end simulations starting from a Gaussian electron beam pulse shape are discussed here, in comparison with the nominal working point performances of a 10ps flat top pulse with rise time of 1ps [1]. Machine parameters have been optimized for the Gaussian pulse shaping both for the standard operating conditions and for the radio-frequency (RF) compressor configuration. In particular, compression factors (C) 2 and 4 have been studied in details. Simulations have been performed using the codes PARMELA [2] and GENESIS [3], for the beam transport along the photoinjector and for the FEL/SASE process respectively.

The two pulse shapes we considered, Gaussian and rectangular with rise time of 1 ps, provide the same saturation length and average power of radiation emitted in the undulator, but the higher current in the beam core of the Gaussian pulse gives a higher peak radiation power at the cost of a broader radiation spectrum. These simulations were performed to investigate thoroughly one of the possible operating modes of the SPARC laser system, which naturally produces such Gaussian shaped pulses.

INTRODUCTION

A longitudinally Gaussian charge distribution has been considered as a possible pulse shaping for the SPARC photoinjector. We optimized the machine free parameters for this pulse shape with a $\sigma_{rms}=2.89$ ps and studied in details this selected working point.

Since the Gaussian time profile exhibits a better linear behavior in the longitudinal space charge field w.r.t. the flat-top profile, we decided to investigate the emittance, energy spread and longitudinal emittance of Gaussian temporal distributions. So we investigated if the emittance and energy spread values could be reduced by taking into consideration an initially Gaussian pulse.

Plots of fig. 1 show that the longitudinal phase space is more linear in the core of the Gaussian profile (right) than for the rectangular case (left), but tails are longer in the first case. However, at this longitudinal position, the correlated energy spread is slightly lower for the Gaussian profile, and the corresponding longitudinal emittance is 34.0 µm, compared to 61.5 µm of the nominal rectangular case. The different characteristics of the two beam distributions are presented below. Furthermore, the chosen Gaussian pulse has been RF compressed, the dynamics of the chirped beam and the FEL/SASE predictions are discussed.
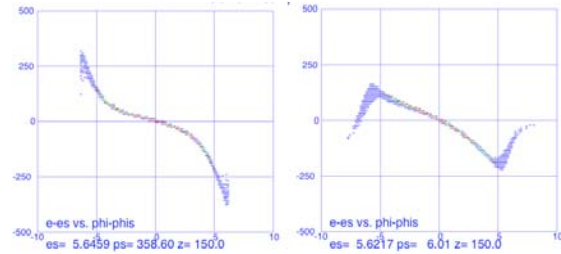

Figure 1: Longitudinal phase space at z=150 cm, the accelerating sections entrance. Left: 10 ps beam pulse and 1 ps rise time (defined as the time interval from 10% to 90% of the total pulse height); right: Gaussian pulse. Energy spread is 1.78% and 1.53% for the rectangular and Gaussian pulse, respectively.

In order to preserve the matching conditions with the beamline we take a Gaussian with the same σ_{rms} of the nominal rectangular pulse of bunch length L=10 ps. So, as the σ_{rms} of a square pulse is given by $L/\sqrt{12}$, we consider a Gaussian temporal pulse with a width of $\sigma=2.89$ ps. This assumption implies that the Gaussian beam has a 40% higher peak current. In fact, the bunch current for the rectangular and Gaussian profiles are respectively given by the following relations:

$$I_{rect} = \frac{\beta cQ}{\pi R^2 L} \quad \text{and} \quad I_{Gaussian} = \frac{\beta cQ}{\pi R^2 \sqrt{2\pi}\sigma_z} e^{-z^2/2\sigma_z^2}$$

so that for the central slice it results that

$$I_{Gaussian} = \sqrt{\frac{6}{\pi}} I_{rect} \approx 1.4 I_{rect}.$$

In principle, this consideration leads to the idea that the high current of the Gaussian beam core pulse could give promising simulation results for the FEL/SASE effects.

Table 1: Parameters that differ for the Gaussian and for the nominal case

	$\varphi_{inj}(°)$	$B_{gun}(T)$	$B_{ITW}(T)$
Nominal	32	0.273	0.615
Gaussian	26	0.271	0.700

OPTIMIZATION OF THE GAUSSIAN WORKING POINT

The set of parameters of the SPARC photoinjector has been fixed by the optimization transport of the nominal pulse shape. We now want to match the Gaussian beam to the beam line, that is we look for a set of parameters such that the longitudinal evolution of the normalized emittance in the gun and drift leads to two relative

minima, and the minimum of the beam envelope corresponds to the relative maximum. The best profile of an electron pulse in relation to the goal of emittance minimization leads to two relative emittance minima which have the same value [4]. This is obtained by a rectangular pulse with zero rise and decay time. The longer the rise time the higher the value of the first minimum and, in turn, the higher the final emittance.
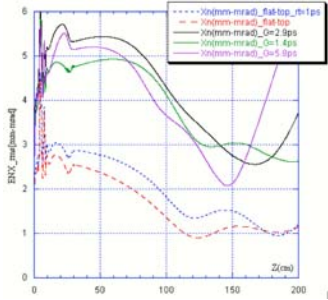

Figure 2: Beam emittance evolution along the first 200 cm of the SPARC injector without accelerating structures for three Gaussian pulses with different width: σ_{rms}=2.89 ps (black curve), σ_{rms}=1.4 ps (green curve) and σ_{rms}=5.8 ps (purple curve), compared to the nominal rectangular pulse with rise time of 1 ps (blue curve) and with no rise time (red curve).

The Gaussian beam evolution along the first 2 m of the injector without accelerating structures is shown by the black curve of fig. 2: the first emittance minimum almost disappears, very similarly to the case of a rectangular pulse shape with long rise time. In this sense we can say that a Gaussian pulse behaves like a rectangular one having long rise times. Moreover, from fig. 2 it can be also be noticed that the symmetry between the two emittance minima behaviour strongly depends on the longitudinal Gaussian width. In fact, the emittance behavior is closer to the rectangular case at the decrease of the Gaussian width (see green curve compared to purple one).
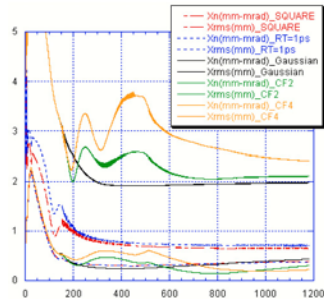

Figure 3: Beam emittance and envelope evolution along the SPARC injector. Black curve is for the Gaussian pulse (σ_{rms}=2.89 ps), compared to the nominal rectangular pulse with rise time of 1 ps (blue curve) and with no rise time (red curve). Green and orange curves represent respectively the C=2 and C=4 with the Gaussian pulse.

For the chosen Gaussian beam with σ_{rms}=2.89 ps, the matching conditions have been optimized by varying the free parameters, that are the gun solenoid field value and

the RF gun injection phase. In table 1 the slight variation values of these two parameters are reported.
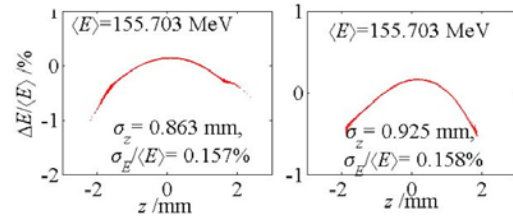

Figure 4: Longitudinal phase space for the Gaussian pulse (*left plot*) and for the nominal case (*right plot*).

Discussing now the beam characteristics at the end of the linac for the two types of initial longitudinal distributions, the longitudinal normalized emittance is ~396 μm and ~438 μm for the Gaussian and for the rectangular pulse, respectively. The rms energy spread is about $\Delta\gamma/\gamma$~0.16% in both cases (see fig. 4). However, the linearity of the Gaussian case permits better energy spread corrections. The normalized emittance is ENX=1.97 μm for the Gaussian shape, much higher than the nominal case (ENX=0.70 μm), as shown in fig. 3.

As for the slice beam properties, in the Gaussian case the slice emittance is about ENX_{slice}~1 μm with a high slice current I_{max}(slice)~130 A, to be compared to the nominal case where most slices have an emittance of ENX_{slice}~0.5 μm and the peak current for the central slice is I_{max}(slice)~110 A (see fig. 5).
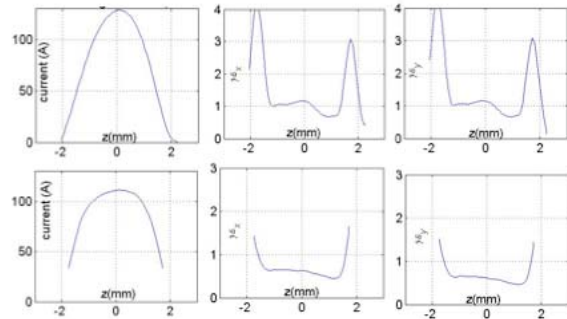

Figure 5: From left to right: slice beam current, slice radial normalized emittance and slice vertical emittance. Upper is for Gaussian case, lower for the nominal one.

FEL/SASE Simulations With the Gaussian Pulse

The slice emittance and energy spread values are good enough for the SASE/FEL process with the chosen Gaussian initial shape through the undulator, at 155 MeV. In fact, the average radiated power calculated for this case predicts saturation within 10 m (black curve of fig. 6). In any case, the photon flux is about 10-15% larger for the nominal profile than for the Gaussian one.

The radiation pulse emitted by the initially Gaussian pulse is shorter but with higher spikes (black curves of fig. 6), if compared to that of the rectangular one [5]. This behavior comes out from the electron beam pulse shape, as in the long Gaussian tails not all the slices are good enough to drive the SASE instability, moreover the beam core gives a 40% higher peak current.

The calculated normalized brightness for the nominal case is $1.1 \cdot 10^{13}$ A/(m rad)^2 and almost a factor 2 lower for the Gaussian case taken into consideration here, essentially due to the higher emittance.
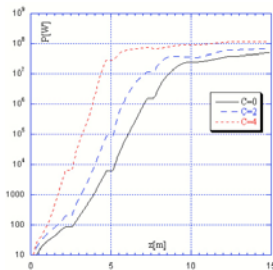

Figure 6: Average radiated power expected for a Gaussian electron beam through the SPARC undulator. The three curves represent: C=0 (black), C=2 (blue) and C=4 (red). For the three cases saturation is predicted.

CHIRPED GAUSSIAN BEAM

The same Gaussian beam pulse discussed above has been chirped with rf compression in the first accelerating section. We present here start to end simulations for the compressor factors C=2 and C=4, where C=σ_z(init)/ σ_z(fin), that is the ratio between initial and final longitudinal σ_{rms}.
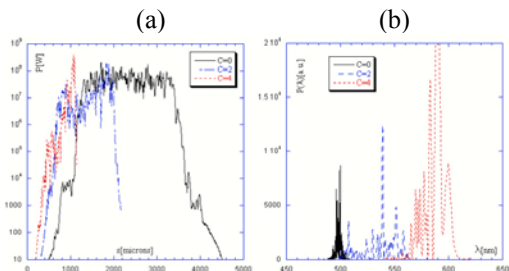

Figure 7: Frame (a) shows the radiation profile at saturation, frame (b) the radiation spectrum at saturation. The three curves represent: C=0 (black), C=2 (blue) and C=4 (red).
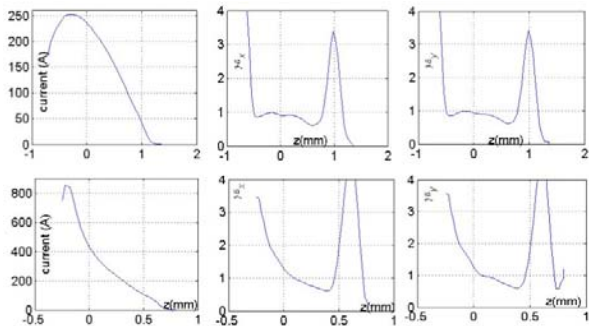

Figure 8: From left to right: slice beam current, slice radial normalized emittance and slice vertical emittance. Upper is for C=2, lower for C=4.

Simulations studies for the C=2 case predict an average beam current of $I_{rms}\sim210$ A. The maximum slice current is I_{max}(slice)~250A and the corresponding slice emittance is ENX$_{slice}\sim0.9$ µm (upper plots of fig. 8). This chirped beam has a rms energy spread of $\Delta\gamma/\gamma\sim1.8\%$, as shown in left plot of fig. 8. The current is higher than I>200A for about ~65% of the beam; the normalized brightness results B=$0.7 \cdot 10^{13}$A/(m rad)^2.

Simulations studies for the C=4 case predict an average beam current of $I_{rms}\sim420$ A. The maximum slice current is I_{max}(slice)~850A and the corresponding slice emittance is ENX$_{slice}\sim3.4$ µm (lower plots of fig. 8). This chirped beam has a rms energy spread of $\Delta\gamma/\gamma\sim1.3\%$, as shown in right plot of fig. 9. The current is higher than I>400A for about ~65% of the beam; the normalized brightness results B=$1.1 \cdot 10^{13}$A/(m rad)^2.
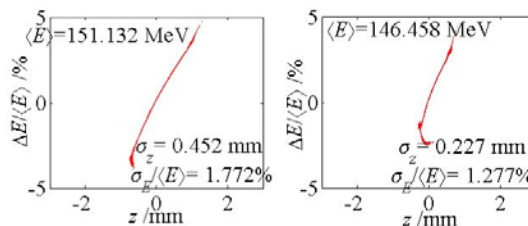

Figure 9: Longitudinal phase space for the Gaussian chirped pulse for C=2 (*left plot*) and C=4 (*right plot*).

As a stronger chirping is taken into account the beam current gets higher at the price of a higher emittance and a more distorted current profile. This behavior is, in turn, transferred to the emitted radiation profile and spectrum. In fact average radiated power increases with the compression factor as shown by the blue (C=2) and red (C=4) curves of fig. 6. However, the stronger the chirping the more distorted is the radiation profile (fig. 7 Frame (a)) and the broader is the radiation spectrum at saturation.

CONCLUSIONS

Start to end simulations for a Gaussian temporal pulse have been performed, finding a parameter set that optimizes its transportation along the linac. FEL/SASE simulations predict about same saturation length but a shorter radiation pulse with higher peak power than for the nominal pulse.

As for the chirped Gaussian beam, the stronger the chirping the higher is the average radiated power and the broader gets the radiation spectrum. Moreover, the radiation profile is more distorted, as it resembles the current profile. This effect can be corrected inserting a higher harmonic cavity, as already verified for the standard working conditions [6].

REFERENCES

[1] D.Alesini et al, "Status of the SPARC Project", EPAC'04, Lucerne, July 2004.
[2] J.Billen, "PARMELA", LA-UR-96-1835,1996.
[3] S.Reiche, *Nucl. Instrum. & Meth.* A429, 243 (1999)
[4] M. Ferrario et al., "Homdyn study for the LCLS Photoinjector", SLAC-PUB-8400, Mar 2000.
[5] M.Boscolo, M.Ferrario, S.Reiche, "Studies of Gaussian Pulse shaping at SPARC", SPARC Techn. Note SPARC-BD-04/002.
[6] C.Ronsivalle et al."Optimization of RF compressor in the SPARX injector", this Conference.